Author Manuscript Published OnlineFirst on July 2, 2021; DOI: 10.1158/0008-5472.CAN-21-0716
Author manuscripts have been peer reviewed and accepted for publication but have not yet been edited.

Quantitative *in vivo* analyses reveal a complex pharmacogenomic landscape in lung adenocarcinoma

Authors

Chuan Li[1,8], Wen-Yang Lin[2,8], Hira Rizvi[3], Hongchen Cai[2], Christopher D. McFarland[1], Zoe N. Rogers[2], Maryam Yousefi[2], Ian P. Winters[2], Charles M. Rudin[4,5], Dmitri A. Petrov[1,6*] and Monte M. Winslow[2,6,7,8*]

Affiliations

[1] Department of Biology, Stanford University, Stanford, CA, USA
[2] Department of Genetics, Stanford University School of Medicine, Stanford, CA, USA
[3] Druckenmiller Center for Lung Cancer Research, Memorial Sloan Kettering Cancer Center, New York, USA
[4] Department of Medicine, Thoracic Oncology Service, Memorial Sloan Kettering Cancer Center, New York, USA
[5] Department of Medicine, Weill Cornell Medical College, New York, USA
[6] Cancer Biology Program, Stanford University School of Medicine, Stanford, CA, USA
[7] Department of Pathology, Stanford University School of Medicine, Stanford, CA, USA
[8] These authors contributed equally

[*] Corresponding authors:
Monte M. Winslow, Stanford University School of Medicine | 279 Campus Drive, Beckman Center, Room B256, Stanford, CA 94305. Phone: 650-725-8696 | Fax: 650-725-1534 | E-mail: mwinslow@stanford.edu

Dmitri A. Petrov, Stanford University | 327 Campus Drive, Bass Biology, Room 232, Stanford, CA 94305
Phone: 650-736-1169 | Fax: 650-723-6132| E-mail: dpetrov@stanford.edu

Running title: Quantifying in vivo pharmacogenomic landscape in lung cancer

Keywords: lung cancer, drug resistance, tumor suppressors, genotype-specific treatment responses

Conflict of interest disclosure statement:

D.A.P., I.P.W, and M.M.W are cofounders of D2G Oncology Inc. D.A.P., I.P.W, Z.N.R, C.D.M, and M.M.W hold equity in D2G Oncology Inc.

Author Manuscript Published OnlineFirst on July 2, 2021; DOI: 10.1158/0008-5472.CAN-21-0716
Author manuscripts have been peer reviewed and accepted for publication but have not yet been edited.

ABSTRACT

The lack of knowledge about the relationship between tumor genotypes and therapeutic responses remains one of the most critical gaps in enabling the effective use of cancer therapies. Here we couple a multiplexed and quantitative experimental platform with robust statistical methods to enable pharmacogenomic mapping of lung cancer treatment responses in vivo. The complex map of genotype-specific treatment responses uncovered that over 20% of possible interactions show significant resistance or sensitivity. Known and novel interactions were identified, and one of these interactions, the resistance of KEAP1 mutant lung tumors to platinum therapy, was validated using a large patient response dataset. These results highlight the broad impact of tumor suppressor genotype on treatment responses and define a strategy to identify the determinants of precision therapies.

Significance: An experimental and analytical framework to generate *in vivo* pharmacogenomic maps that relate tumor genotypes to therapeutic responses reveals a surprisingly complex map of genotype-specific resistance and sensitivity.

INTRODUCTION

Efforts over the past decade have generated many novel cancer therapies(1,2). However, patient responses are heterogeneous, with some patients responding well and others showing limited or no response(3,4). While it is believed that the genetic complexity of cancer underlies a significant portion of the variation in therapeutic response, the map of such pharmacogenomic interactions is currently lacking(5-7). Despite widespread tumor genotyping, only a few driver mutations currently inform clinical treatment decisions and clinical trial designs(8-10). This is driven by the fact that we do not yet know which tumor suppressor alterations influence sensitivity or resistance to specific therapies. The very premise that tumor suppressor genotype substantially impacts therapeutic responses remains largely untested.

The pharmacogenomic landscape of cancer drug responses has been investigated using cell lines, patient-derived xenografts (PDXs), and patient treatment outcome data(5,11-14). However, such genotype-treatment interactions are notoriously difficult to measure using these systems for four major reasons: the large numbers of driver and passenger mutations, the observational instead of manipulative nature of the experiments, lack of the appropriate autochthonous *in vivo* environment, and the high stochasticity of tumor growth. Specifically, cell lines grown *in vitro* lack the appropriate *in vivo* environment, do not represent all cancer subtypes, and often carry additional alterations that arise during passaging(15). PDXs and human cell line transplantation models recapitulate some aspects of *in vivo* growth, but growth factor/receptor incompatibility, growth in non-orthotopic sites, and the obligate absence of the adaptive immune system compromise these approaches(16-18). Furthermore, human tumor-derived systems almost invariably have large numbers of mutations and genomic alterations. Thus, even large-scale analyses often lack the statistical power to glean cause-and-effect relationships between individual genomic alterations and therapeutic responses(5,14). The same logic applies to patient treatment response data, which are generally too limited in scale to provide sufficient statistical power to confidently associate tumor suppressor genotypes with metrics of clinical response(19). Such data are particularly sparse for unapproved therapies (limited to clinical trial results) and are nonexistent for preclinical therapeutic candidates.

A cost-effective system that introduces defined genomic alterations, measures the response of a large number of isogenic tumors, and recapitulates the *in vivo* physiological context could be valuable for uncovering genotype-treatment relationships. Here we present such a system based on tumor-barcoding in genetically engineered mouse models. Genetically engineered mouse models of human cancer are important preclinical models, as they recapitulate the physiological, tissue, and immunological context of tumor growth(20,21). These models uniquely enable the introduction of defined genomic alterations into adult somatic cells, which leads to the generation of autochthonous tumors(20). These tumors can recapitulate the genomic alterations, gene expression state, histopathology, and therapy-refractive nature of corresponding human cancers(11,22). Despite the potential value of these models in preclinical translation studies, the breadth of their utility has been limited in practice by the fact that they are neither readily scalable nor sufficiently quantitative(23-27).

To increase the scope and precision of *in vivo* cancer modeling and to assess tumor suppressor gene function in a multiplexed manner, we previously developed a system that couples tumor-barcoding with high-throughput barcode sequencing (Tuba-seq)(26). This method integrates CRISPR/Cas9-based somatic genome engineering and molecular barcoding into well-established Cre/Lox-based genetically engineered mouse models of oncogenic Kras-driven lung cancer(28). The initiation of lung tumors with pools of barcoded Lenti-sgRNA/Cre viral vectors enables the generation of many tumors of different genotypes in parallel. All neoplastic cells within each clonal tumor have the same two-component barcode, in which an sgID region identifies the sgRNA and a random barcode (BC) is unique to each tumor. Thus, high-throughput sequencing of the sgID-BC region from bulk tumor-bearing lungs can quantify the number of neoplastic cells in each tumor of each genotype(28). Previous Tuba-seq studies quantify tumor suppressor effects and their interaction with other tumor suppressor genes, focusing only on comparisons *within* mice(28-30). Comparisons of tumor distributions *across* mice are more challenging and required improvements in accuracy as well as new analytical methods.

Author Manuscript Published OnlineFirst on July 2, 2021; DOI: 10.1158/0008-5472.CAN-21-0716
Author manuscripts have been peer reviewed and accepted for publication but have not yet been edited.

Here, we optimize multiple key aspects of the Tuba-seq approach. The greatly improved accuracy in tumor calling enabled us to compare tumor size distributions between groups of mice, *i.e.*, treated and untreated groups, and to generate a large-scale map that relates tumor genotype to therapeutic responses *in vivo*. We developed a new analytical and computational framework, Pharmacogenomic tumor barcoding with high-throughput barcode sequencing (PGx-Tuba-seq). We quantify the treatment responses of tens of thousands of oncogenic KRAS-driven lung tumors of eleven different tumor suppressor genotypes to a diverse panel of therapies, and uncover a surprisingly complex pharmacogenomic map of resistance and sensitivity. PGx-Tuba-seq represents a more tractable method to uncover the therapeutic response of different tumor genotypes than previous *in vitro* and *in vivo* screening approaches.

MATERIALS AND METHODS

Mice, tumor initiation, and drug treatment

All animal experiments have been approved by Institutional Animal Care at Stanford University with protocol number 26696. Lung tumors were initiated by intratracheal delivery of the same lentiviral pools(26). 1.1 x 10^5 and 2.2 x 10^4 infectious unit/mouse were administered to each $Kras^{LSL\text{-}G12D}$ *(K), R26*$^{LSL\text{-}Tomato}$ *(T)*(hereafter *KT*), and *KT;H11*$^{LSL\text{-}Cas9}$ mouse(31-33), respectively. Drug treatments were started 15 weeks after tumor initiation. For the main pharmacogenomic mapping experiment, mice were assigned to eight treatment arms or were left untreated for 3 weeks (**Fig. 1a**, **Table 1**).

Tuba-seq library generation

Genomic DNA was isolated from bulk tumor-bearing lung tissue from each mouse(26). Three benchmark control cell lines (~5x10^5 cells/cell line) were added to each mouse lung sample prior to lysis to enable the calculation of the absolute cancer cell number within each tumor(28). To reduce the errors of the Tuba-seq pipeline from orders of magnitudes, we implemented multiple critical changes to the library preparation, sequencing, and analysis (**Table 2-3**). Q5 High-Fidelity 2x Master Mix (NEB, M0494X) was used to amplify the sgID-BC region from 32 µg of genomic DNA(34). To improve sequencing quality, we used unique dual-indexed primers and added 6-9 random nucleotides (Ns) to the flanking ends of both index primers before the sequence-specific primer regions(35). The libraries were pooled based on lung weight to ensure even reading depth and sequenced on an Illumina HiSeq 2500 platform (Admera Health) with paired-end 150 bp reads.

Processing reads to identify the sgID and barcode and removal of "spurious tumor" generated by read errors

We required both the forward and reverse sequencing reads to match perfectly within the BC region. FASTQ files were processed to identify the sgID and BC counts for each tumor. The sgID region identified the targeted tumor suppressor gene. The number of reads with each unique sgID-BC in each sample was summed to calculate each putative tumor's size. PCR and sequencing errors within the random barcode regions may be misinterpreted as unique tumors. We used stringent criteria to reduce and even eliminate the effects of PCR and sequencing errors on tumor calls, greatly reducing the spurious tumor (**Fig. 1b, Supplementary Fig. 1a**) when quantifying relative tumor sizes (**Fig. 1c, Supplementary Fig. 1b-d**), showing larger effect sizes (**Supplementary Fig. 2a-d**).

Author Manuscript Published OnlineFirst on July 2, 2021; DOI: 10.1158/0008-5472.CAN-21-0716
Author manuscripts have been peer reviewed and accepted for publication but have not yet been edited.

Developing unbiased procedures for detecting genotype-specific drug effects

Previous Tuba-seq analyses focused on comparing the sizes of tumors of different genotypes within individual mice (28,30). Such analyses are largely robust to multiple sources of variation among mice (**Supplementary Fig. 3a-d**). We needed to compare tumor sizes between the untreated and the treated group when analyzing genotype-specific drug responses. We used the same viral pool to initiate tumors in all mice, therefore the relative representation of transduced epithelial cells containing each Lenti-sgRNA/Cre is constant and does not vary across mice.

Null model of tumor responses with no genotype-specificity

We assume that the therapy affects all tumors proportionally to their sizes such that the size of each tumor changes from X to $X_1 = X \times S$ after the treatment, where S is the proportion of remaining cancer cells. Under the null model (H_0) of no genotype-specific drug responses, S is constant and does not depend on tumor genotype. Under the alternative model H_1, S varies depending on the genotype: $S_{sgID,\, j} = S_{Inert}\times(1+G_j)$, with G_j representing the Genotype Specific Therapeutic Response (GSTR) of tumors of specific genotypes to the drug j. If $G_j > 0$, the inactivation of the tumor suppressor gene confers relative resistance; if $G_j < 0$, the inactivation of the tumor suppressor gene confers relative sensitivity.

The most extreme treatment reduced tumor sizes by ~87%. While the depth of sequencing varied across mice and treatments, we wanted to reliably identify tumors in each treated and untreated mouse. Thus, we chose to use the cutoff of L = 1000 cells in the untreated mice, allowing reliable detection and accurate size estimates of tumors in each mouse.

Author Manuscript Published OnlineFirst on July 2, 2021; DOI: 10.1158/0008-5472.CAN-21-0716
Author manuscripts have been peer reviewed and accepted for publication but have not yet been edited.

Calculation of proportional size-reduction as the drug effect

To estimate the value of the tumor reduction factor *S* that leads to the best match between the distributions of Inert tumors between the treated and untreated group, we calculated the value of *S* such that the median number of shrunk tumors across all the untreated mice was closest to the median of the number of observed tumors with the size above or equal to 1000 cells across all the mice in the treated group.

Using relative tumor number (*ScoreRTN*) to estimate GSTR

Our first approach defines response as the number of tumors that exceed a minimum size threshold (**Fig. 2a, b**). The null hypothesis for each genotype is that the number of tumors above the cutoff *L* in the untreated mice should match the number above the new cutoff *L*×S in the treated mice. If a GSTR exists, the tumors with a specific sgID are more resistant to the drug than the Inert tumors, and more of such tumors should remain above the adjusted cutoff of *L*×*S* than expected, while if they are more sensitive, fewer such tumors should remain above the adjusted cutoff of *L*×*S*. We first calculate the ratio of the number of tumors above the cutoff *L* in the untreated mice of a particular sgID to that of the Inert tumors ($RTN_{i,j,L}$),

$$RTN_{i,j=untreated,L} = \frac{\sum_k \mathrm{C}_{i,\mathrm{j=untreated,k}}}{\sum_k \mathrm{C}_{Inert,\mathrm{j=untreated,k}}}$$

$$for\ all\ mice\ k\ and\ all\ tumors\ equal\ or\ larger\ than\ L$$

where $C_{i,j,k}$ is the total number of tumors observed in mouse *k* in treatment group *j* (*j* = untreated here) carrying sgID *i* above the cutoff *L*. We then calculate the similar ratio for the treated mice with a modified cutoff *L*×*S*,

Author Manuscript Published OnlineFirst on July 2, 2021; DOI: 10.1158/0008-5472.CAN-21-0716
Author manuscripts have been peer reviewed and accepted for publication but have not yet been edited.

$$RTN_{i,j,L\times S} = \frac{\sum_k \mathrm{C}_{i,\mathrm{j,k}}}{\sum_k \mathrm{C}_{Inert,\mathrm{j,k}}} \; for\ all\ mice\ k\ and\ all\ tumors\ larger\ than\ L \times S$$

The null hypothesis can then be expressed as the expectation that

$$RTN_{i,untreated,L} = RTN_{i,j,L\times S}$$

or alternatively that:

$$ScoreRTN_{i,j} = log_2\left(\frac{RTN_{i,j,L\times S}}{RTN_{i,Untreated,L}}\right) = 0$$

Under the alternative hypothesis where $ScoreRTN_{i,j} \neq 0$, a positive sign of $ScoreRTN_{i,j}$ suggests that the tumors with a particular sgID are more resistant than the Inert tumors, while a negative sign suggests the tumors are more sensitive than Inert tumors.

Use relative geometric mean (*ScoreRGM*) to estimate GSTR

The second metric, Score*RGM*, compares the geometric mean of tumors carrying sgID *i* relative to the Inert tumors in the untreated and treated groups (**Fig. 2a, c**). If we analyze a comparable number of tumors in the untreated and treated mice, with no *GSTR*, the relative growth advantage of tumors carrying a specific sgID (sgID *i*) relative to Inert tumors, represented by the relative geometric mean, will remain constant. If the tumors with a specific sgID (sgID *i*) are resistant to the drug, the relative geometric mean for sgID *i* will be larger in the treated group, while if sensitive, the relative geometric mean will be smaller. While *RTN* does not use the numeric value of tumor size other than comparing it with the cutoff, *RGM* incorporates such tumor size profile information. Hence, *RGM* and *RTN* are not entirely redundant as they incorporate different information about *GSTR*.

We denote the total tumor count (*T*) with a certain sgRNA (*i*) in an individual mouse (*k*) in the treated group (*j*) as $T_{i,j,k}$. Here, we do not limit tumors to those above 1000 cells but rather count any tumor with greater than or equal to 2 reads (after the stringent filtering described above) as a tumor. For an untreated mouse, the proportion of initiated tumors of each sgID can be approximated by R_i, the ratio of $T_{i,untreated,k}$ to $T_{Inert,untreated,k}$:

$$R_i = \text{median}\left(\frac{T_{i,untreated,k}}{T_{Inert,untreated,k}} \middle| for\ all\ \ mice\ k\right)$$

We then take the top N tumors with sgRNA i from mouse k treated by drug j as:

$$\mathrm{N}_{i,j,k} = \mathrm{C}_{i,j,k} \times \mathrm{R}_i$$

where $C_{i,j,k}$ is the total number of Inert tumors observed in each mouse above the cutoff $L \times S$ (S=1 for the untreated group), and then we calculate the geometric mean for all tumors containing the sgID and Inert tumors across all mice in the group.

The score for the relative geometric mean is calculated as:

$$ScoreRGM_{i,j} = Log_2\left(\frac{\mathrm{GM_{i,j}} / \mathrm{GM_{Inert,j}}}{\mathrm{GM_{i,untreated}} / \mathrm{GM_{Inert,untreated}}}\right)$$

where $\mathrm{GM_{i,j}}$ is the geometric mean for tumors containing sgID i in treatment group j in the selected N tumors. Under the null hypothesis, $ScoreRGM_{i,j} = 0$. Under the alternative hypothesis where $ScoreRGM_{i,j} \neq 0$, a positive sign of $ScoreRGM_{i,j}$ suggests that the tumors with a particular sgID are more resistant than the Inert tumors, while a negative sign of the score suggests that these tumors are more sensitive than the Inert tumors.

Calculating ScoreGSTR ($\widehat{G}$) as the combined score

Although *ScoreRTN* and *ScoreRGM* may have an emphasis on different aspects of *GSTR* on tumor size distribution, it is helpful to have a single combined score. We calculated a combined score of GSTR ($\hat{G}$) by taking the inverse variance weighted average of *ScoreRTN* and *ScoreRGM*, then converting it to the linear scale (**Fig. 3).**

$$ScoreGSTR = \left(\frac{ScoreRTN}{\sigma^2_{ScoreRTN}} + \frac{ScoreRGM}{\sigma^2_{ScoreRGM}}\right) / \left(\frac{1}{\sigma^2_{ScoreRTN}} + \frac{1}{\sigma^2_{ScoreRGM}}\right)$$

$$\hat{G} = 2^{ScoreGSTR} - 1$$

If $\hat{G}>0$, *GSTR* is resistant, and if $\hat{G}<0$, *GSTR* is sensitive.

To be conservative, for the combined score to be called significant, we require at least one significant *P*-value ($P < 0.05$), and one marginally significant *P*-value ($P < 0.1$) for the two statistics *ScoreRTN* and *ScoreRGM*.

Comparing with human cell line response database GDSC

The drug sensitivity data from human cell lines were downloaded from the Genomics of Drug Sensitivity in Cancer (GDSC) database (www.cancerrxgene.org)(5). Due to the limited number of LUAD cell lines, we focused on comparing the results from Pan-cancer cell lines. All 5 monotherapies used in our study were assessed by GDSC. Except for *Keap1* and *Rbm10*, which are not reported for everolimus and paclitaxel, the GSTR of all other 51 gene-drug pairs were quantified by GDSC. The effect size and FDR-corrected *P*-values were used for comparison.

Analysis of clinical data for resistance to chemotherapy

Despite relatively widespread genotyping, clinical treatment data and response data are extremely limited. MSKCC has a tremendous program to genotype patients and to collect clinical data. Most patients with oncogenic KRAS-driven lung cancer get platinum doublet therapy as no targeted therapies have been approved. Patients with metastatic or recurrent lung adenocarcinoma harboring a KRAS mutation in codons 11, 12, or 61, as detected by MSK-IMPACT (36), were reviewed. Patients who received platinum chemotherapy (carboplatin or cisplatin) with pemetrexed +/- bevacizumab as first-line treatment were included (n = 216). Treatment efficacy was measured as time of first treatment with platinum doublet chemotherapy to start of next systemic therapy, or death if no subsequent therapy was received. Patients who continued on platinum doublet therapy at the last follow-up were censored. The retrospective chart review was approved by the MSK institutional review board.

Kaplan-Meier estimator plots of time-to-next-treatment for patients with and without mutations at each of the 11 tumor suppressor genes of interest were generated. In addition, a multivariable Cox proportional hazards model analysis was performed, integrating the mutational status of the 11 genes as individual input features to assess the independent effect of co-occurring mutations.

Data availability statement

The sequencing dataset generated and analyzed during the current study is available in the Gene Expression Omnibus database (accession code: GSE146448). Other data and relevant code are available in https://github.com/lichuan199010/Tuba-seq-analysis-and-summary-statistics.

RESULTS

Development of the PGx-Tuba-seq pipeline

To eliminate sgRNA-sgID/barcode uncoupling due to lentiviral template switching and to minimize PCR, sequencing, and clustering errors, we made multiple improvements to our Tuba-seq experimental protocols and analysis pipeline (**Fig. 1a, Table 2-3,** and **Methods**)(26). We initiated lung tumors in *Kras*$^{LSL\text{-}G12D/+}$;*Rosa26*$^{LSL\text{-}Tomato}$;*H11*$^{LSL\text{-}Cas9}$ (*KT;H11*$^{LSL\text{-}Cas9}$) mice and control Cas9-negative *KT* mice with a pool of barcoded Lenti-sgRNA/Cre vectors targeting eleven putative tumor suppressors and four control vectors with inert sgRNAs (Lenti-sg*TS*^{Pool}/Cre; **Fig. 1a**). To eliminate template switching during lentiviral reverse transcription, we generated each vector separately and pooled each viral vector immediately prior to tumor initiation(37). Tumor suppressors were selected based on common occurrence in human lung adenocarcinomas and previously suggested roles in oncogenesis(26). 18 weeks after tumor initiation, the sgID-BC region from each bulk tumor-bearing lung was PCR amplified and sequenced to quantify the number of neoplastic cells in each tumor (**Fig. 1a**).

Our new analysis pipeline essentially eliminated the impact of read errors, as assessed by two metrics, including the spurious tumors generated from spike-in barcodes with known sequences and correspondence of tumor barcodes with those from the lentiviral plasmid pool (**Fig. 1b**, **Supplementary Fig. 1a**). Quantification of the impact of tumor suppressor gene inactivation on tumor growth in *KT;H11*$^{LSL\text{-}Cas9}$ mice using our optimized method uncovered effects that were generally consistent with our previous analyses, but with greater magnitudes of tumor suppression (**Fig. 1c**; **Supplementary Fig. 1c, d** and **2a-d**; sign test for differences in magnitudes, P = 0.001)(28). Consistent with the robustness of our methods, analysis of the *KT* mice with Lenti-sg*TS*^{Pool}/Cre-initiated tumor revealed no false-positive tumor suppressive effects (**Supplementary Fig. 1c, d**). These technical improvements to the Tuba-seq method further enhance the ability of this technology to be applied to study a variety of questions in tumor progression and evolution, as well as quantification of the pharmacogenomic interactions as performed in this study.

Author Manuscript Published OnlineFirst on July 2, 2021; DOI: 10.1158/0008-5472.CAN-21-0716
Author manuscripts have been peer reviewed and accepted for publication but have not yet been edited.

When quantifying tumor suppressor gene effects using Tuba-seq, each mouse represents an internally-controlled experiment in which metrics of tumor size can be compared between tumors of each tumor suppressor genotype and tumors initiated with inert sgRNAs within the same mouse (**Fig. 1c, Supplementary Fig. 1b-d**)(26). In contrast, comparing tumor size distributions between groups of mice, such as between untreated and drug-treated groups, requires methods that address the technical and biological differences among mice. To understand the statistical properties and potential biases intrinsic to this type of analysis, we rigorously modeled drug responses and genotype-specific responses. We initially performed our modeling with the assumption that cancer cells in tumors of all sizes respond equally to each treatment, while the treatment effects can vary by genotype. Specifically, we estimated the drug effect on control tumors (those with inert sgRNAs) and then applied this effect to all tumors to calculate an expected distribution of tumor sizes after treatment (**Fig. 2a** and **Methods**). Genotype-specific therapeutic responses (GSTRs) were quantified by comparing the observed distribution of tumor sizes for tumors of a certain genotype after treatment with the expected distribution derived from the untreated mice. We developed two statistics to characterize GSTRs: (1) *ScoreRTN* – Relative Tumor Number, which compares the relative numbers of tumors above a certain size after treatment; and (2) *ScoreRGM* – Relative Geometric Mean, which constitutes the relative change in the geometric mean of tumors from the full distribution of tumor sizes (**Methods**). By assessing the performance of the two statistics, we showed that both statistics are unbiased (**Supplementary Fig. 3e-h**) and exhibit substantial and similar power (**Supplementary Fig. 4a-c**), although one statistic may outperform the other if the genotype-specific response is not uniform across tumor sizes (**Methods, Fig. 2b-c** and **Supplementary Fig. 5a, b**). Moreover, by performing power analysis and plotting the ROC curves for both statistics across multiple

Author Manuscript Published OnlineFirst on July 2, 2021; DOI: 10.1158/0008-5472.CAN-21-0716
Author manuscripts have been peer reviewed and accepted for publication but have not yet been edited.

sample sizes (*i.e.,* number of mice/group), we confirmed the high sensitivity and specificity of our system (**Fig. 2b, c** and **Supplementary Fig. 4a-c**). We also found that relaxing the assumption that tumors of all sizes respond proportionally to treatment did not change our results substantially (**Supplementary Fig. 5a-b**).

Complex pharmacogenomic map uncovered using the PGx-Tuba-seq pipeline

We applied Tuba-seq and our statistical metrics to assess the genotype-specific therapeutic responses of 11 genotypes of lung tumors to a panel of eight single and combination therapies (**Fig. 1a, Fig. 3a,** and **Table 1**). These therapies were chosen to perturb diverse signaling pathways and assess the genotype-dependency of chemotherapy responses. *KT;H11$^{LSL\text{-}Cas9}$* mice with Lenti-sg*TS^{Pool}*/Cre-initiated lung tumors were treated for three weeks with one of the eight therapies followed by Tuba-seq analysis (**Fig. 1a** and **Fig. 3a**). The total cancer cell numbers estimated by Tuba-seq were highly correlated with total tumor-bearing lung weights, which varied substantially among mice even within the same groups (**Supplementary Fig. 6a-c)**. Despite expected mouse-to-mouse variations, comparing the overall tumor burden and the number of tumors with inert sgRNAs in the untreated and treated mice revealed significant overall therapeutic effects for five out of the eight treatments (**Supplementary Fig. 6d**).

We compared the tumor size profiles of treated mice with those of untreated mice and calculated the *ScoreRTN* and *ScoreRGM* (**Supplementary Fig. 7a**). For both statistics, we estimated the magnitudes of genotype-specific therapeutic responses (GSTRs) and the associated *P*-values using bootstrapping. Across all genotypes and treatments, the two statistics were well-correlated in magnitude as expected under the model of proportional tumor responses (**Supplementary Fig. 7b;** $r = 0.86$, $P{=}10^{-46}$). Among the 88 assessed genotype-treatment pairs,

Author Manuscript Published OnlineFirst on July 2, 2021; DOI: 10.1158/0008-5472.CAN-21-0716
Author manuscripts have been peer reviewed and accepted for publication but have not yet been edited.

20 and 17 significant GSTRs (P < 0.05) were identified by *ScoreRTN* and *ScoreRGM*, respectively. Of these, 19 genotype-treatment interactions were significant by one statistic (P < 0.05) and at least marginally significant (P < 0.1) by the other (**Supplementary Fig. 7a, b; Table S1**). We derived a composite measure of GSTR ($\hat{G}$) with the magnitude estimated from the inverse variance weighted average of the two statistics (**Methods**, **Fig. 3b**). Analysis of genotype-specific effects across treatments highlighted similarities among tumor suppressors, including those of Lkb1 and Setd2 that we have previously suggest to have redundant tumor suppressive effects[5]. Furthermore, combination treatments clustered with their corresponding single therapies (**Supplementary Fig. 7c, d**), and an additive model shows good predictive power (**Supplementary Fig. 7e, f**). Power analysis showed that our findings were robust to the cancer cell number cutoff (**Supplementary Fig. 8a**), choice of inert sgRNAs (**Supplementary Fig. 8b**), and inaccurate estimation of drug effects (**Supplementary Fig. 9a, b**).

One of the detected GSTRs was well known in advance – the resistance of Rb1-deficient tumors to the CDK4/6 inhibitor, palbociclib. Our ability to rediscover this interaction serves as a positive control of our method and is consistent with the expectation that some pharmacogenomic interactions transcend cancer types (**Supplementary Fig 10a-e**). This resistance is consistent with the biochemical features of this pathway (**Supplementary Fig. 10f**) and clinical findings in breast cancer and hepatocellular carcinoma(38-40).

To further test the performance of our experimental and statistical procedures, we performed two additional experiments. First, as a negative control for GSTR identification, we treated Cas9-negative *KT* mice with a combination of chemotherapy and Mek-inhibition (**Supplementary Fig. 11a**). This treatment led to a dramatic reduction in tumor sizes compared to untreated *KT* mice (**Supplementary Fig. 11b**). Only one false positive GSTR was identified

Author Manuscript Published OnlineFirst on July 2, 2021; DOI: 10.1158/0008-5472.CAN-21-0716
Author manuscripts have been peer reviewed and accepted for publication but have not yet been edited.

(*ScoreRTN*, P = 0.03; *ScoreRGM*, P = 0.07) with a very weak magnitude of the effect ($\hat{G}$ = 0.093, while the minimum magnitude of significant GSTR interactions in the main experiment was 0.108; **Fig. 3c**, **Supplementary Fig. 11c**). Furthermore, none of the individual inert sgRNAs (sg*Neo1*, sg*Neo2*, sg*Neo3*, and sg*NT*) had a significant effect by either metric for any of the eight treatments in our main pharmacogenomic mapping experiment, adding confidence in the veracity of the detected GSTRs (**Fig. 3b**, **c**).

Simulations suggest that these cohort sizes have substantial albeit imperfect power (**Supplementary Fig. 4a-c**); therefore, we next attempted to rediscover the genotype-palbociclib interactions. We initiated tumors in a similar, yet somewhat smaller cohort of $KT;H11^{LSL\text{-}Cas9}$ mice with Lenti-sgTS^{Pool}/Cre and repeated the palbociclib treatment. Analyses of these mice again identified *Rb1* inactivation as a mediator of palbociclib resistance (**Fig. 3d, Supplementary Fig. 10b**). *Smad4*-deficient tumors, which showed modest resistance in our initial experiment, showed nominal resistance in the repeat experiment ($\hat{G}$ = 0.167), although this interaction was not significant (P = 0.17 and 0.20 for *ScoreRTN* and *ScoreRGM*, respectively). Given the magnitude of this GSTR and our sample sizes, this false negative is not surprising. Assuming a true positive rate of 80%, which is considered desirable(41,42), when identifying two genuine GSTR signals (*Smad4* and *Rb1*, for instance) in two independent experiments, the probability of missing at least one of these findings is $1\text{-}80\%^4$=59%.

Multiple sources of evidence confirm the findings of our PGx-Tuba-seq analysis

Although most of the detected pharmacogenomic interactions we uncovered are novel, several lines of evidence derived from clinical and preclinical data are consistent with our observations. For instance, *Lkb1*-inactivation reduced sensitivity to mTOR inhibition in our data,

Author Manuscript Published OnlineFirst on July 2, 2021; DOI: 10.1158/0008-5472.CAN-21-0716
Author manuscripts have been peer reviewed and accepted for publication but have not yet been edited.

which is supported by a previous *in vitro* study(43) and anecdotal data from the analysis of lung adenocarcinoma patient-derived primary cultures (**Supplementary Fig. 12a-c**)(12). Moreover, previous studies have shown that *Kras*^{G12D}*;Lkb1*$^{-/-}$ lung tumors are sensitive to phenformin(25) and resistant to MEK inhibition(23).

The ultimate goal of our study was to find genotype-treatment responses that predicted lung adenocarcinoma patient responses. Lung adenocarcinoma patients are often treated with first-line platinum-containing combination therapies. In our analysis, *Keap1*-inactivation led to resistance to treatments that included carboplatin, while not promoting significant resistance to the other therapies (**Fig. 3b**). Interestingly, Keap1-inactivation has been previously suggested to reduce responses to chemotherapy(44-46). To further investigate the clinical impact of tumor suppressor genotype on lung adenocarcinoma responses, we queried the tumor suppressor genotype and therapeutic benefit of platinum-containing treatments (assessed as time-to-next-treatment) of 216 patients with oncogenic *KRAS*-driven human lung adenocarcinomas treated at Memorial Sloan Kettering Cancer Center (**Methods**). When each gene was assessed individually (**Supplementary Fig. 13a-k**), both *KEAP1* and *LKB1* mutations were associated with worse clinical outcomes (P=6×10^{-6}, **Fig. 4a** and P = 0.06, **Supplementary Fig. 13c, j**, respectively). However, the marginally significant effect of *LKB1* mutation appears to be driven primarily by the co-occurrence of *KEAP1* and *LKB1* mutations(47,48) (**Supplementary Fig. 13l)**. This finding is also well supported by our pharmacogenomic data in which *Lkb1*-inactivation did not confer resistance to platinum-containing treatments (**Fig. 3b**). We further quantified the hazard ratio of the mutational status of the 11 genes accounting for the effect of other co-incident mutations. This analysis confirmed that mutations of *KEAP1* correlated with a shorter time-to-next-treatment, which is consistent with our Tuba-seq results as well as a previous study on the

Author Manuscript Published OnlineFirst on July 2, 2021; DOI: 10.1158/0008-5472.CAN-21-0716
Author manuscripts have been peer reviewed and accepted for publication but have not yet been edited.

impact of *KEAP1/NRF2*-pathway alterations on platinum responses (**Fig. 4a, b**)(44,49). Our *in vivo* pharmacogenomic platform, in which the responses of tumors with defined genotypes can be quantified, establishes direct causal relationships between genotype and treatment responses, and enables accurate interpretation of patient data.

Comparisons with the cell line and PDX data

While the positive and negative predictive values of cancer cell line studies are often questioned(50), the scale at which these *in vitro* studies can be performed has enabled the generation of drug response data across large panels of cell lines(11,51,52). Our study constitutes the largest *in vivo* survey of GSTRs, thus we compared our findings to a study of cell line-therapeutic responses (Genomics of Drug Sensitivity in Cancer; GDSC)(5) in which all five of our monotherapies were assessed (paclitaxel, palbociclib, phenformin, everolimus/rapamycin, and trametinib)(5). Among the genotype-treatment pairs assessed in both studies, nine had significant effects in our analysis, but only one of these genotype-treatment pairs was significant in GDSC (*RB1*-palbociclib; **Fig. 4c-d** and **Supplementary Fig. 14a, b**). Note that in general we would not expect excellent agreement between our results and the cell line studies, given the lack of the autochthonous environment as well as the complexity of genetic backgrounds and mutation load in cell lines(50,53).

The PRISM/DepMap compound screen has also quantified genotype-specific treatment responses(54). We tested whether mutation of each tumor suppressor gene is associated with a better or worse response for each genotype-treatment pair (the Mann-Whitney U-test with FDR-correction). The log viability measured by PRISM/DepMap compound screen and *ScoreGSTR* predicted by Tubaseq were significantly correlated ($\rho = 0.34$, $P = 0.01$). Among the 9 significant genotype-treatment pairs predicted by Tuba-seq, 7 of them are in the same direction in the PRISM/DepMap compound screen dataset, although only three of these effects were significant in PRISM (**Table S2**). This is likely driven in part by their small sample size and the fact that in the PRISM/DepMap compound screen dataset, the results are correlative and ignore all co-occurring mutations, while our analysis establishes a direct causal relationship.

Patient-derived tumor xenograft models (PDX) can also be used to test for the association between genotype and drug response. Gao *et al.* conducted a very broad PDX study, generating a total of 4759 response curves from ~1000 PDXs treated with 62 treatments (**Table S3**)(55). We used two-way ANOVA to determine whether there are any significant genotype-treatment pairs in these PDX data where the therapies overlap with our Tuba-seq results. Overall, there was no significant correlation between our *ScoreGSTR* and these ANOVA results ($r = 0.124$, $P = 0.623$; $\rho = 0.07$, $P = 0.792$, **Table S4**). Given the large number of mutations per PDX (642 on average for the cancers used for comparison) and the small number of response curves measured per gene-drug pair (median number of treated PDXs that have the gene of interest mutated was 6, see **Table S3**), the lack of correlation is not surprising. This PDX study, despite its extremely large scope, failed to identify the positive control genotype-treatment pair of *RB1*-mutated tumors being resistant to CDK4/6 inhibitors. These PDX results also did not uncover that *KEAP1* inactivation leads to resistance to chemotherapy, which is an interaction that has been confirmed with clinical data (**Fig. 4a**)(44).

DISCUSSION

Here we described and validated a scalable and quantitative *in vivo* pharmacogenomic preclinical model, which has high power to identify genotype-treatment responses using modest-size cohorts of mice. While the number of mice required is modest, the total number of assayed

Author Manuscript Published OnlineFirst on July 2, 2021; DOI: 10.1158/0008-5472.CAN-21-0716
Author manuscripts have been peer reviewed and accepted for publication but have not yet been edited.

tumors is large – on the order of thousands per mouse – providing the ability to assay a large number of tumor suppressors in the same experiment at a reasonable cost (**Supplementary Fig. 15a-c**). Indeed, while genetically engineered mouse models are key preclinical models to study genotype-specific treatment responses, traditional approaches are neither rigorously quantitative nor scalable, requiring impractically large numbers of mice. For instance, we estimated that with ten mice per group, the sensitivity of our approach would be > 99% to detect a genotype-specific treatment resistance that results in tumor sizes that are 50% larger than control tumors. If we had used a more traditional approach of comparing four cohorts of mice (with and without a specific tumor-suppressor alteration and therapy-treated versus vehicle-treated), ~300 mice/group would be required to achieve the same sensitivity for just one tumor suppressor genotype (**Supplementary Fig. 15a-c**). To build the pharmacogenomic map presented in this study, we would have needed to breed, initiate tumors in, and treat ~10,000 mice instead of 58; thus, our system represents a >100-fold increase in throughput. Moreover, our power to detect effects is mostly limited by the number of mice per group and not by the number of tumors per mouse, allowing future iterations of this approach to query more genotypes per mouse.

We used one sgRNA per gene for the screening, and one may be concerned with the efficiency and off-target effects of the sgRNA. However, these sgRNAs has been extensively validated by previous studies. The ruggedness of the pharmacogenomic landscape further suggests the efficiency of the sgRNAs, with seven out of the 11 sgRNAs showed some genotype-specific treatment responses. Moreover, our pipeline is largely immune to off-target effects for sgRNAs, and such effects would not be expected to generate GSTRs (**Supplementary Fig. 3** and **Supplemental Methods and Discussion**). Furthermore, neither differences in tumor number nor overall tumor burden across mice dramatically shift tumor suppressive effects, suggesting that this methods is not dramatically influence by mouse-to-mouse variation (**Supplementary Fig. 16a-b**)(29).

Our method is not only scalable and quantitative, but also allows the introduction of specific alterations into each tumor and the study of *marginal* effects of individual tumor suppressor genes in isolation which is not possible using traditional cell line or PDX approaches. Moreover, the use of genetically engineered mouse models allows autochthonous tumors to develop in their natural immunocompetent environment. This provides the ability to study immunotherapies but also the ability to recapitulate aspects of chemotherapy and targeted therapy responses that are influence by adaptive immune responses.

The key result of this study, which had been suspected but never directly demonstrated, is that tumor suppressor genotype has a substantial impact on responses to a range of distinct therapies. The fact that this was not previously demonstrated experimentally is primarily due to the lack of appropriate systems, which underscores the need for higher-throughput quantitative preclinical models(27). Indeed, while databases like TCGA and GENIE databases provide valuable information on the mutational spectra in tumors, these databases generally lack treatment histories and cannot be used to study pharmacogenomic interactions. Prior cell-line studies suggested that very few genotypes significantly impact drug responses (e.g., 0.24% of genotype-treatment pairs in GDSC), which we believe is largely due to the lack of statistical power. In contrast, we show that >20% of genotype-treatment pairs show interactions, suggesting a complex pharmacogenomic map of resistance and sensitivity of *KRAS*-driven lung adenocarcinoma.

There are some potential caveats for our PGx-Tuba-seq approach. We can only introduce a limited number of mutations into each tumor, reducing our ability to recapitulate the high tumor mutation burden and overall complexity of human tumors. While we can study the genetic interaction among up to three genes, is it possible that even higher order interactions could modify the pharmacogenomic landscape. Furthermore, the extent to which our results recapitulate reponses in patients remains unknown due to the lack of large-scale patient data sets. Thus, the interpretation of our results will benefit from further experimental, bioinformatic and clinical evidence.

The complexity and rugged nature of this pharmacogenomic map has important implications for precision medicine. The complexity of human cancer genomics and the large number of potential therapies suggest that large-scale investigation of the pharmacogenomic maps in preclinical models will aid in patient selection. Our framework for *in vivo* functional genomic studies should easily allow larger number of genes and additional monotherapies and combination therapies to be tested. Application to other genomic sub-types of lung cancer and potentially to other cancer types should further increase our knowledge of the pharmacogenomic determinants of therapy responses(56). We anticipate that the use of this platform to quantify the effects of additional therapies across a greater diversity of cancer genotypes will provide a cause-and-effect pharmacogenomic understanding from which novel biological hypotheses and precision treatment approaches will emerge.

Acknowledgements:

We thank L. Andrejka for technical support; A. Orantes and S. Mello for administrative support; members of the Stanford Animal care staff for excellent animal care; D. Feldser, J. Sage, J. Zhang, and members of the Winslow and Petrov laboratories for helpful comments. C. Li was the Connie and Bob Lurie Fellow of the Damon Runyon Cancer Research Foundation

(DRG-2331). W-Y. Lin was supported by an American Association of Cancer Research Postdoctoral fellowship (17-40-18-LIN). H. Rizvi was supported by the Druckenmiller Center for Lung Cancer Research at MSK. H. Cai was supported by a Tobacco-Related Disease Research Program Postdoctoral Fellowship (28FT-0019). C.D. McFarland was supported by NIH K99-CA226506. M. Yousefi was supported by a Stanford Dean's fellowship, an American Lung Association senior research training grant, and NIH F32-CA236311. I.P. Winters was supported by the NSF Graduate Research Fellowship Program and NIH F31-CA210627. This work was supported by NIH R01-CA207133 (to M.M. Winslow and D.A. Petrov), NIH R01-CA231253 (to M.M. Winslow and D.A. Petrov), NIH R01-CA234349 (to M.M. Winslow and D.A. Petrov) and NIH U01-CA199215 (C.M. Rudin).

AUTHOR CONTRIBUTIONS

C.L., W-Y.L., C.M.R., D.A.P., and M.M.W. planned the project. C.L. performed bioinformatics and statistical analysis. W-Y.L., H.C., M.M.W., Z.R., and M.Y. performed the mouse experiments. H.R. collected the patient response dataset. H.R. and C.L. analyzed the human dataset. Z.N.R., I.P.W., and C.D.M. assisted with mouse experiments. C.L., W-Y.L., M.M.W, and D.A.P. wrote the paper.

References

1. Miller KD, Nogueira L, Mariotto AB, Rowland JH, Yabroff KR, Alfano CM*, et al.* Cancer treatment and survivorship statistics, 2019. CA Cancer J Clin **2019**;69:363-85
2. Denisenko TV, Budkevich IN, Zhivotovsky B. Cell death-based treatment of lung adenocarcinoma. Cell Death Dis **2018**;9:117

3. Dagogo-Jack I, Shaw AT. Tumour heterogeneity and resistance to cancer therapies. Nat Rev Clin Oncol **2018**;15:81-94
4. Bedard PL, Hansen AR, Ratain MJ, Siu LL. Tumour heterogeneity in the clinic. Nature **2013**;501:355-64
5. Iorio F, Knijnenburg TA, Vis DJ, Bignell GR, Menden MP, Schubert M*, et al.* A Landscape of Pharmacogenomic Interactions in Cancer. Cell **2016**;166:740-54
6. Wang Y, Wang Z, Xu J, Li J, Li S, Zhang M*, et al.* Systematic identification of non-coding pharmacogenomic landscape in cancer. Nat Commun **2018**;9:3192
7. Qiu Z, Li H, Zhang Z, Zhu Z, He S, Wang X*, et al.* A Pharmacogenomic Landscape in Human Liver Cancers. Cancer Cell **2019**;36:179-93 e11
8. Wood DE, Kazerooni EA, Baum SL, Eapen GA, Ettinger DS, Hou L*, et al.* Lung Cancer Screening, Version 3.2018, NCCN Clinical Practice Guidelines in Oncology. J Natl Compr Canc Netw **2018**;16:412-41
9. Ettinger DS, Wood DE, Aisner DL, Akerley W, Bauman J, Chirieac LR*, et al.* Non-Small Cell Lung Cancer, Version 5.2017, NCCN Clinical Practice Guidelines in Oncology. J Natl Compr Canc Netw **2017**;15:504-35
10. Punt CJ, Koopman M, Vermeulen L. From tumour heterogeneity to advances in precision treatment of colorectal cancer. Nat Rev Clin Oncol **2017**;14:235-46
11. Barretina J, Caponigro G, Stransky N, Venkatesan K, Margolin AA, Kim S*, et al.* The Cancer Cell Line Encyclopedia enables predictive modelling of anticancer drug sensitivity. Nature **2012**;483:603-7
12. Lee JK, Liu Z, Sa JK, Shin S, Wang J, Bordyuh M*, et al.* Pharmacogenomic landscape of patient-derived tumor cells informs precision oncology therapy. Nat Genet **2018**;50:1399-411
13. Roper N, Stensland KD, Hendricks R, Galsky MD. The landscape of precision cancer medicine clinical trials in the United States. Cancer Treat Rev **2015**;41:385-90
14. Gao H, Korn JM, Ferretti S, Monahan JE, Wang Y, Singh M*, et al.* High-throughput screening using patient-derived tumor xenografts to predict clinical trial drug response. **2015**;21:1318
15. Ben-David U, Siranosian B, Ha G, Tang H, Oren Y, Hinohara K*, et al.* Genetic and transcriptional evolution alters cancer cell line drug response. Nature **2018**;560:325-30
16. Hidalgo M, Amant F, Biankin AV, Budinska E, Byrne AT, Caldas C*, et al.* Patient-Derived Xenograft Models: An Emerging Platform for Translational Cancer Research. Cancer discovery **2014**;4:998-1013
17. Ben-David U, Ha G, Tseng YY, Greenwald NF, Oh C, Shih J*, et al.* Patient-derived xenografts undergo mouse-specific tumor evolution. Nat Genet **2017**;49:1567-75
18. Hoffman RMJNRC. Patient-derived orthotopic xenografts: better mimic of metastasis than subcutaneous xenografts. **2015**;15:451
19. Middleton G, Fletcher P, Popat S, Savage J, Summers Y, Greystoke A*, et al.* The National Lung Matrix Trial of personalized therapy in lung cancer. Nature **2020**;583:807-12
20. Kersten K, de Visser KE, van Miltenburg MH, Jonkers J. Genetically engineered mouse models in oncology research and cancer medicine. EMBO Mol Med **2017**;9:137-53
21. Sharpless NE, Depinho RA. The mighty mouse: genetically engineered mouse models in cancer drug development. Nat Rev Drug Discov **2006**;5:741-54

22. Singh M, Murriel CL, Johnson LJCr. Genetically engineered mouse models: closing the gap between preclinical data and trial outcomes. **2012**;72:2695-700
23. Chen Z, Cheng K, Walton Z, Wang Y, Ebi H, Shimamura T*, et al.* A murine lung cancer co-clinical trial identifies genetic modifiers of therapeutic response. Nature **2012**;483:613-7
24. Schmitt A, Knittel G, Welcker D, Yang T-P, George J, Nowak M*, et al.* ATM deficiency is associated with sensitivity to PARP1-and ATR inhibitors in lung adenocarcinoma. **2017**;77:3040-56
25. Shackelford DB, Abt E, Gerken L, Vasquez DS, Seki A, Leblanc M*, et al.* LKB1 inactivation dictates therapeutic response of non-small cell lung cancer to the metabolism drug phenformin. Cancer Cell **2013**;23:143-58
26. Rogers ZN, McFarland CD, Winters IP, Naranjo S, Chuang CH, Petrov D*, et al.* A quantitative and multiplexed approach to uncover the fitness landscape of tumor suppression in vivo. Nat Methods **2017**;14:737-42
27. Winters IP, Murray CW, Winslow MM. Towards quantitative and multiplexed in vivo functional cancer genomics. Nat Rev Genet **2018**;19:741-55
28. Rogers ZN, McFarland CD, Winters IP, Seoane JA, Brady JJ, Yoon S*, et al.* Mapping the in vivo fitness landscape of lung adenocarcinoma tumor suppression in mice. Nat Genet **2018**;50:483-6
29. Cai H, Chew SK, Li C, Tsai MK, Andrejka L, Murray CW*, et al.* A functional taxonomy of tumor suppression in oncogenic KRAS-driven lung cancer. Cancer discovery **2021**
30. Murray CW, Brady JJ, Tsai MK, Li C, Winters IP, Tang R*, et al.* An LKB1-SIK Axis Suppresses Lung Tumor Growth and Controls Differentiation. Cancer discovery **2019**;9:1590-605
31. Jackson EL, Willis N, Mercer K, Bronson RT, Crowley D, Montoya R*, et al.* Analysis of lung tumor initiation and progression using conditional expression of oncogenic K-ras. **2001**;15:3243-8
32. Chiou SH, Winters IP, Wang J, Naranjo S, Dudgeon C, Tamburini FB*, et al.* Pancreatic cancer modeling using retrograde viral vector delivery and in vivo CRISPR/Cas9-mediated somatic genome editing. Genes Dev **2015**;29:1576-85
33. Madisen L, Zwingman TA, Sunkin SM, Oh SW, Zariwala HA, Gu H*, et al.* A robust and high-throughput Cre reporting and characterization system for the whole mouse brain. Nat Neurosci **2010**;13:133-40
34. Pezza JA, Kucera R, Sun LJNEB. Polymerase fidelity: what is it, and what does it mean for your PCR. **2014**
35. MacConaill LE, Burns RT, Nag A, Coleman HA, Slevin MK, Giorda K*, et al.* Unique, dual-indexed sequencing adapters with UMIs effectively eliminate index cross-talk and significantly improve sensitivity of massively parallel sequencing. BMC Genomics **2018**;19:30
36. Cheng DT, Mitchell TN, Zehir A, Shah RH, Benayed R, Syed A*, et al.* Memorial Sloan Kettering-Integrated Mutation Profiling of Actionable Cancer Targets (MSK-IMPACT): A Hybridization Capture-Based Next-Generation Sequencing Clinical Assay for Solid Tumor Molecular Oncology. J Mol Diagn **2015**;17:251-64
37. Hill AJ, McFaline-Figueroa JL, Starita LM, Gasperini MJ, Matreyek KA, Packer J*, et al.* On the design of CRISPR-based single-cell molecular screens. Nat Methods **2018**;15:271-4

38. Bollard J, Miguela V, Ruiz de Galarreta M, Venkatesh A, Bian CB, Roberto MP*, et al.* Palbociclib (PD-0332991), a selective CDK4/6 inhibitor, restricts tumour growth in preclinical models of hepatocellular carcinoma. Gut **2017**;66:1286-96
39. Knudsen ES, Pruitt SC, Hershberger PA, Witkiewicz AK, Goodrich DW. Cell Cycle and Beyond: Exploiting New RB1 Controlled Mechanisms for Cancer Therapy. Trends Cancer **2019**;5:308-24
40. O'Leary B, Cutts RJ, Liu Y, Hrebien S, Huang X, Fenwick K*, et al.* The Genetic Landscape and Clonal Evolution of Breast Cancer Resistance to Palbociclib plus Fulvestrant in the PALOMA-3 Trial. Cancer discovery **2018**;8:1390-403
41. Hong EP, Park JW. Sample size and statistical power calculation in genetic association studies. Genomics Inform **2012**;10:117-22
42. Wittes J. Sample size calculations for randomized controlled trials. Epidemiol Rev **2002**;24:39-53
43. Xiao P, Sun LL, Wang J, Han RL, Ma Q, Zhong DS. LKB1 gene inactivation does not sensitize non-small cell lung cancer cells to mTOR inhibitors in vitro. Acta Pharmacol Sin **2015**;36:1107-12
44. Arbour KC, Jordan E, Kim HR, Dienstag J, Yu HA, Sanchez-Vega F*, et al.* Effects of Co-occurring Genomic Alterations on Outcomes in Patients with KRAS-Mutant Non-Small Cell Lung Cancer. Clin Cancer Res **2018**;24:334-40
45. Zhang P, Singh A, Yegnasubramanian S, Esopi D, Kombairaju P, Bodas M*, et al.* Loss of Kelch-like ECH-associated protein 1 function in prostate cancer cells causes chemoresistance and radioresistance and promotes tumor growth. Mol Cancer Ther **2010**;9:336-46
46. Tian Y, Wu K, Liu Q, Han N, Zhang L, Chu Q*, et al.* Modification of platinum sensitivity by KEAP1/NRF2 signals in non-small cell lung cancer. J Hematol Oncol **2016**;9:83
47. Galan-Cobo A, Sitthideatphaiboon P, Qu X, Poteete A, Pisegna MA, Tong P*, et al.* LKB1 and KEAP1/NRF2 Pathways Cooperatively Promote Metabolic Reprogramming with Enhanced Glutamine Dependence in KRAS-Mutant Lung Adenocarcinoma. Cancer Res **2019**;79:3251-67
48. Papillon-Cavanagh S, Doshi P, Dobrin R, Szustakowski J, Walsh AM. STK11 and KEAP1 mutations as prognostic biomarkers in an observational real-world lung adenocarcinoma cohort. ESMO Open **2020**;5
49. Jeong Y, Hellyer JA, Stehr H, Hoang NT, Niu X, Das M*, et al.* Role of KEAP1/NFE2L2 Mutations in the Chemotherapeutic Response of Patients with Non-Small Cell Lung Cancer. Clin Cancer Res **2019**
50. Haibe-Kains B, El-Hachem N, Birkbak NJ, Jin AC, Beck AH, Aerts HJ*, et al.* Inconsistency in large pharmacogenomic studies. Nature **2013**;504:389-93
51. Garnett MJ, Edelman EJ, Heidorn SJ, Greenman CD, Dastur A, Lau KW*, et al.* Systematic identification of genomic markers of drug sensitivity in cancer cells. Nature **2012**;483:570-5
52. Corsello SM, Nagari RT, Spangler RD, Rossen J, Kocak M, Bryan JG*, et al.* Discovering the anticancer potential of non-oncology drugs by systematic viability profiling. **2020**;1:235-48

53. Bouhaddou M, DiStefano MS, Riesel EA, Carrasco E, Holzapfel HY, Jones DC*, et al.* Drug response consistency in CCLE and CGP. Nature **2016**;540:E9-E10
54. Corsello SM, Nagari RT, Spangler RD, Rossen J, Kocak M, Bryan JG*, et al.* Discovering the anti-cancer potential of non-oncology drugs by systematic viability profiling. Nat Cancer **2020**;1:235-48
55. Gao H, Korn JM, Ferretti S, Monahan JE, Wang Y, Singh M*, et al.* High-throughput screening using patient-derived tumor xenografts to predict clinical trial drug response. Nat Med **2015**;21:1318-25
56. Foggetti G, Li C, Cai H, Hellyer JA, Lin WY, Ayeni D*, et al.* Genetic determinants of EGFR-Driven Lung Cancer Growth and Therapeutic Response In Vivo. Cancer discovery **2021**

Author Manuscript Published OnlineFirst on July 2, 2021; DOI: 10.1158/0008-5472.CAN-21-0716
Author manuscripts have been peer reviewed and accepted for publication but have not yet been edited.

Table 1. Treatments tested using the PGx-Tuba-seq platform.

Type	Treatment	Dose	Frequency	Route of administration
Monotherapy	Palbociclib	100 mg/kg	Daily	Oral gavage
Monotherapy	Everolimus	10 mg/kg	Daily	Oral gavage
Monotherapy	Phenformin	100 mg/kg	Daily	Oral gavage
Monotherapy	Paclitaxel	20 mg/kg	Every other day	Intraperitoneal injection
Monotherapy	Trametinib	0.3 mg/kg	Daily	Oral gavage
Combination	Paclitaxel + Trametinib	20 mg/kg 0.3 mg/kg	Every other day Daily	Intraperitoneal injection Oral gavage
Combination	Carboplatin + Paclitaxel	50 mg/kg 20 mg/kg	Every five days Every other day	Intraperitoneal injection Intraperitoneal injection
Combination	Carboplatin + Paclitaxel + Trametinib	50 mg/kg 20 mg/kg 0.3 mg/kg	Every five days Every other day Daily	Intraperitoneal injection Intraperitoneal injection Oral gavage

Author Manuscript Published OnlineFirst on July 2, 2021; DOI: 10.1158/0008-5472.CAN-21-0716

Table 2. Overview of our optimized Tuba-seq analysis pipeline for calling sgID-BCs from sequencing data and determining the number of neoplastic cells in each tumor

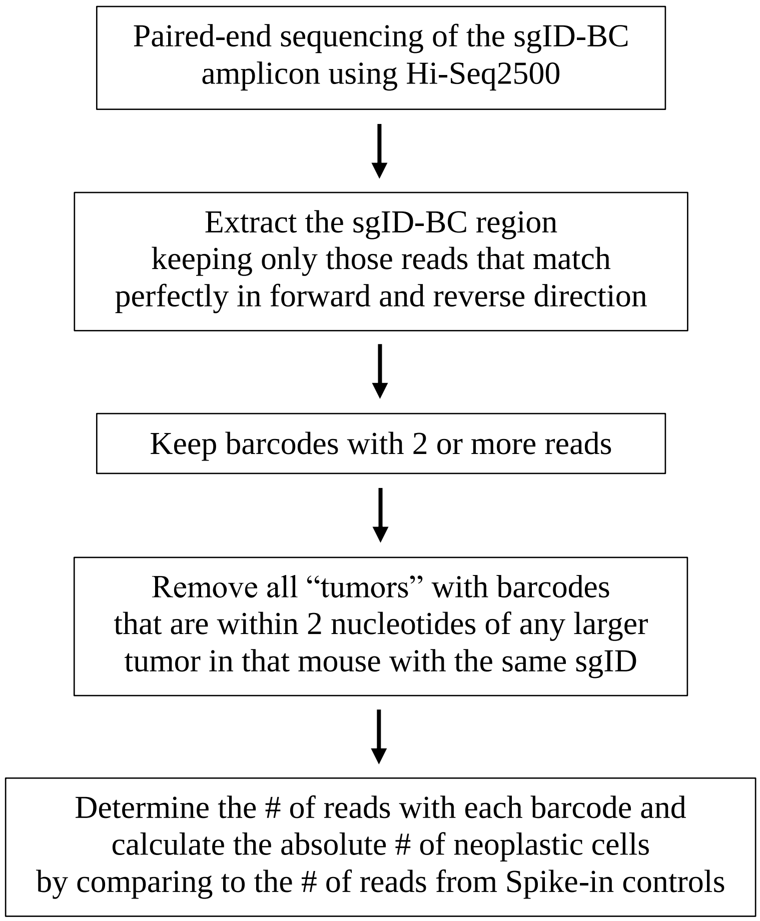

Author Manuscript Published OnlineFirst on July 2, 2021; DOI: 10.1158/0008-5472.CAN-21-0716
Author manuscripts have been peer reviewed and accepted for publication but have not yet been edited.

Table 3. Comparison of our current pipeline with our previous Tuba-seq pipeline

Module	**Previous (Rogers *et al.*, 2017)**	**Current**	**Purpose**
Viral production	Pooled	Each viral vector was prepared separately	Eliminate Lentiviral template switching
Library preparation	Taq polymerase	Q5 polymerase	Reduce PCR errors
Library preparation	Single indexing	Dual unique indexing	Eliminate the impact of index hopping during sequencing on tumor calling
Sequencing	Single-end	Paired-end	Reduce “spurious tumors” created by sequencing errors
Read processing and tumor calling	DADA2 clustering	Stringent filtering on reads Remove spurious tumors recursively based on hamming distance	Eliminate “spurious tumors” created by PCR and sequencing errors
Read processing and tumor calling	No restriction on BC length	Require exact length match	Eliminate “spurious tumors” created by PCR and sequencing errors

FIGURE LEGENDS

Figure 1. Optimization of tumor-barcoding coupled with high-throughput barcode sequencing (Tuba-seq) for the analysis of genotype-specific therapy responses (GSTRs) *in vivo*.

a. Overview of Tuba-seq pipeline to uncover GSTRs. The Lenti-TS$^{\mathrm{Pool}}$/Cre viral pool contains barcoded vectors with sgRNAs targeting 11 putative tumor suppressors that are frequently mutated in human lung adenocarcinoma. Tumors are initiated in either $Kras^{LSL\text{-}G12D/+}$;$R26^{LSL\text{-}Tom}$ (*KT*) or $Kras^{LSL\text{-}G12D/+}$;$R26^{LSL\text{-}Tom}$;$H11^{LSL\text{-}Cas9}$ (*KT*;$H11^{LSL\text{-}Cas9}$) mice. Following tumor development, mice are treated with therapies, and barcode sequencing libraries are prepared from each tumor-bearing lung. Multiple technical advances in the pipeline involve viral production, library preparation, sequencing and analysis pipeline have been made, boosting the accuracy of our pipeline to enable many further applications.

b. Stringent filtering effectively eliminated spurious tumors. Analysis of the barcodes associated with the sgID specific for the Spike-in control cells (3 cell lines with a defined sgID-BC added at $5\text{x}10^5$ cell/sample as the benchmark) enables identification of recurrent barcode reads generated from sequencing and other errors (Spurious tumors). Data is from a typical lane of 22 multiplexed Tuba-seq libraries from *KT*;$H11^{LSL\text{-}Cas9}$ mice with Lenti-TS$^{\mathrm{Pool}}$/Cre initiated tumors.

c. The relative size of tumors of each genotype in *KT*;$H11^{LSL\text{-}Cas9}$ mice 18 weeks after tumor initiation with Lenti-sgTS$^{\mathrm{Pool}}$/Cre. The relative sizes of tumors at the indicated percentiles were calculated from the tumor size distribution of all tumors in 5 mice. Error bars show 95% confidence intervals.

Figure 2. Tuba-seq is a powerful tool to quantify genotype-specific therapeutic responses (GSTR).

a. Data analysis pipeline to identify GSTR by comparing the relative tumor number (*ScoreRTN*) and relative geometric mean (*ScoreRGM*) between tumors containing a tumor suppressor targeting sgRNA and Inert tumors in the untreated and treated mice.

b. A receiver operating characteristic curve showing the sensitivity and specificity of *ScoreRTN* estimated from simulations of preassigned drug effect (S=0.5) and GSTR (various G) using 8 untreated mice and 5 treated mice. There is no genotype-specific response when G=0. G of -20% means the tumors with the sgRNA were reduced by an additional 20% in size.

c. A receiver operating characteristic curve showing the sensitivity and specificity of *ScoreRGM* estimated from the same simulation as in b.

Figure 3. Tuba-seq quantifies genotype-specific therapeutic responses (GSTR) to multiple therapies.

a. Timeline of the experiment. Tumors were initiated in $KT;H11^{LSL\text{-}Cas9}$ mice with the barcoded Lenti-sgTS^{Pool}/Cre. Three weeks of treatment was initiated after 15 weeks of tumor growth. The number of mice used for each treatment arm is shown.

b-d. The estimated genotype-specific treatment response($\hat{G}$) calculated from the inverse variance weighted average of *ScoreRTN* and *ScoreRGM* for the pharmacogenomic mapping experiment (**b**), negative control experiment in *KT* mice (**c**), and palbociclib repeat experiment (**d**). Stars represent significant effects.

Figure 4. Comparison of Tuba-seq identified GSTRs with cell line and clinical data.

a. Kaplan-Meier curve (with 95% confidence interval in shading) of time-to-next-treatment (months) for patients with or without *KEAP1* mutations with metastatic oncogenic *KRAS*-driven lung adenocarcinoma to platinum-containing chemotherapy. The number of patients in each group is shown. *P*-values were calculated from the Mantel-Haenszel test.

b. Responses of patients with metastatic oncogenic *KRAS*-driven lung adenocarcinoma to platinum-containing chemotherapy are consistent with *KEAP1* inactivation leading to resistance. *KEAP1* mutations are significantly correlated with a higher hazard ratio for time-to-next-treatment.

Author Manuscript Published OnlineFirst on July 2, 2021; DOI: 10.1158/0008-5472.CAN-21-0716
Author manuscripts have been peer reviewed and accepted for publication but have not yet been edited.

c. Correlation between GSTR estimated in our study and that from the Genomics of Drug Sensitivity in Cancer (GDSC) database based on cancer cell line studies. The significant GSTRs in our study are highlighted in red.

d. Comparison of our identified GSTRs with data from the GDSC database. Stars represent significant cases.

Author Manuscript Published OnlineFirst on July 2, 2021; DOI: 10.1158/0008-5472.CAN-21-0716
Author manuscripts have been peer reviewed and accepted for publication but have not yet been edited.

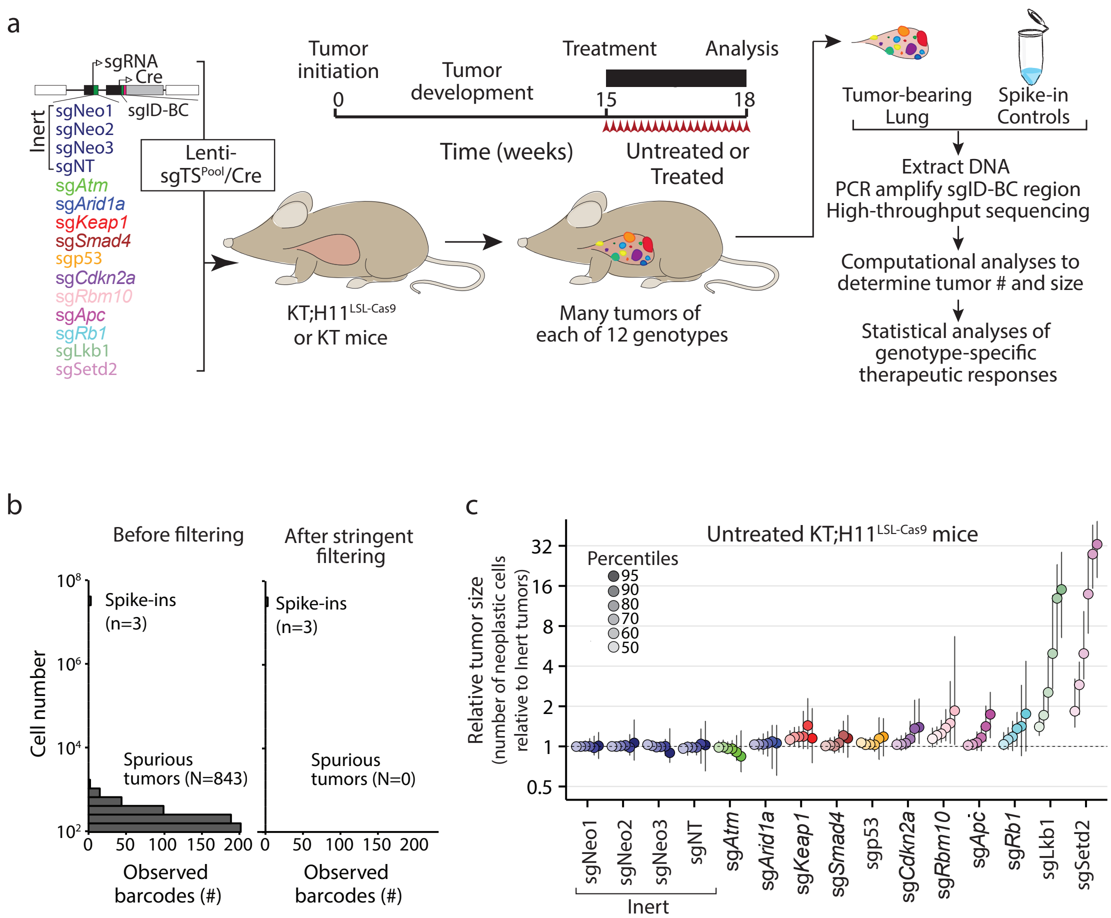

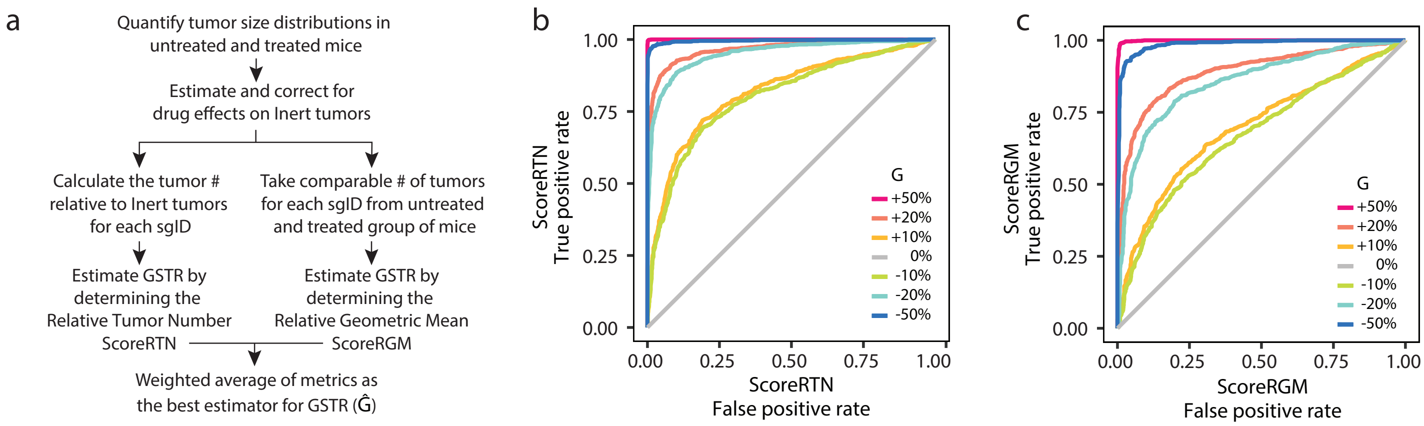
a
Quantify tumor size distributions in untreated and treated mice
Estimate and correct for drug effects on Inert tumors
Calculate the tumor # relative to Inert tumors for each sgID
Take comparable # of tumors for each sgID from untreated and treated group of mice
Estimate GSTR by determining the Relative Tumor Number
ScoreRTN
Estimate GSTR by determining the Relative Geometric Mean
ScoreRGM
Weighted average of metrics as the best estimator for GSTR (Ĝ)
b
ScoreRTN
True positive rate
ScoreRTN
False positive rate
0.00
0.25
0.50
0.75
1.00
G
+50%
+20%
+10%
0%
-10%
-20%
-50%
c
ScoreRGM
True positive rate
ScoreRGM
False positive rate
G
+50%
+20%
+10%
0%
-10%
-20%
-50%

Figure 2

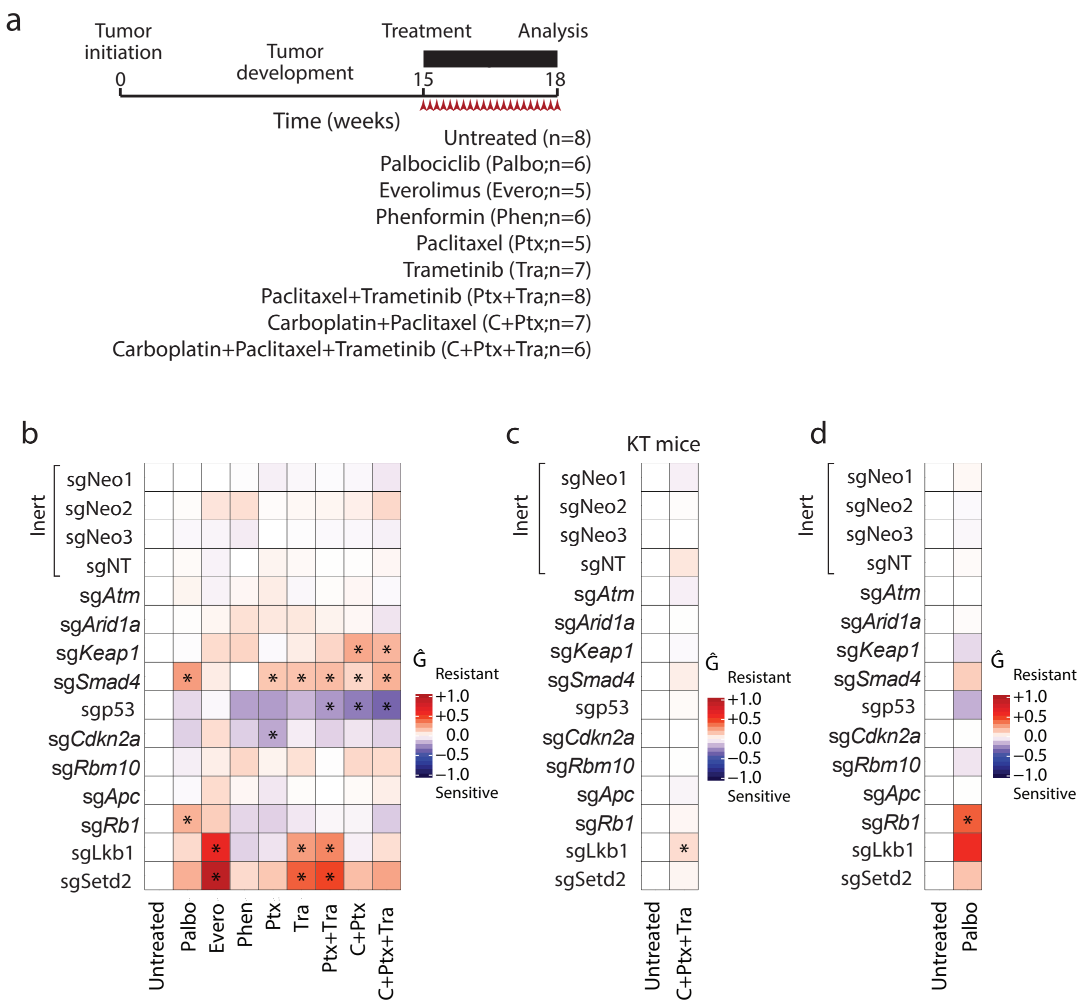
a
Tumor initiation
Tumor development
Treatment
Analysis
0
15
18
Time (weeks)
Untreated (n=8)
Palbociclib (Palbo;n=6)
Everolimus (Evero;n=5)
Phenformin (Phen;n=6)
Paclitaxel (Ptx;n=5)
Trametinib (Tra;n=7)
Paclitaxel+Trametinib (Ptx+Tra;n=8)
Carboplatin+Paclitaxel (C+Ptx;n=7)
Carboplatin+Paclitaxel+Trametinib (C+Ptx+Tra;n=6)
b
c
KT mice
d
Inert
sgNeo1
sgNeo2
sgNeo3
sgNT
sgAtm
sgArid1a
sgKeap1
sgSmad4
sgp53
sgCdkn2a
sgRbm10
sgApc
sgRb1
sgLkb1
sgSetd2
Untreated
Palbo
Evero
Phen
Ptx
Tra
Ptx+Tra
C+Ptx
C+Ptx+Tra
Ĝ
Resistant
+1.0
+0.5
0.0
−0.5
−1.0
Sensitive

Figure 3

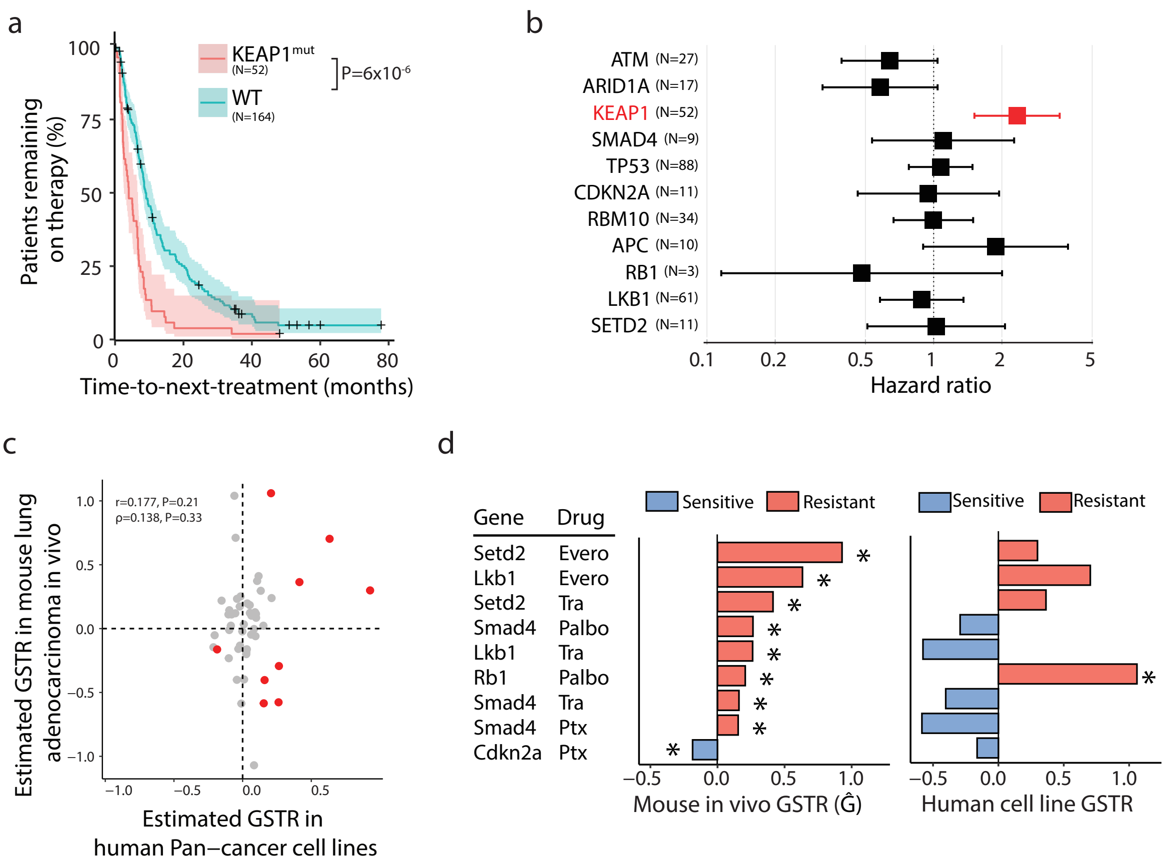
a
Patients remaining on therapy (%)
Time-to-next-treatment (months)
KEAP1mut (N=52)
WT (N=164)
P=6x10-6
b
ATM (N=27)
ARID1A (N=17)
KEAP1 (N=52)
SMAD4 (N=9)
TP53 (N=88)
CDKN2A (N=11)
RBM10 (N=34)
APC (N=10)
RB1 (N=3)
LKB1 (N=61)
SETD2 (N=11)
Hazard ratio
c
r=0.177, P=0.21
ρ=0.138, P=0.33
Estimated GSTR in mouse lung adenocarcinoma in vivo
Estimated GSTR in human Pan−cancer cell lines
d
Gene
Drug
Sensitive
Resistant
Setd2 Evero
Lkb1 Evero
Setd2 Tra
Smad4 Palbo
Lkb1 Tra
Rb1 Palbo
Smad4 Tra
Smad4 Ptx
Cdkn2a Ptx
Mouse in vivo GSTR (Ĝ)
Human cell line GSTR

Figure 4

Author Manuscript Published OnlineFirst on July 2, 2021; DOI: 10.1158/0008-5472.CAN-21-0716
Author manuscripts have been peer reviewed and accepted for publication but have not yet been edited.

Cancer Research
The Journal of Cancer Research (1916–1930) | The American Journal of Cancer (1931–1940)

American Association for Cancer Research

Quantitative in vivo analyses reveal a complex pharmacogenomic landscape in lung adenocarcinoma

Chuan Li, Wen-Yang Lin, Hira Rizvi, et al.

Cancer Res Published OnlineFirst July 2, 2021.